

Supplementary materials for "One-dimensional Lieb superlattices: from the discrete to the continuum limit"

Dylan Jones,^a Marcin Mucha-Kruczynski,^a Adelina Ilie^a and Lucian Covaci^{b,c}

^a Department of Physics, University of Bath, Bath, UK

^b Department of Physics, University of Antwerp, Antwerp, Belgium.

^c NANOLight Center of Excellence, University of Antwerp, Antwerp, Belgium.

S1 Projection onto the anisotropic Dirac cone (ADC)

To project the original Lieb SL TB Hamiltonian H onto the ADC crossing point, we need the unitary transformation $\tilde{H} = UHU^\dagger$ that gives

$$\tilde{H} = \begin{bmatrix} H_0 & T \\ T^\dagger & H_1 \end{bmatrix}, \quad (\text{S.1})$$

where H_0 is a 2×2 zero-eigenvalue block at the ADC crossing. To find the unitary matrix U , the wave function is expressed in a new basis where the first two components are a set, prescribed linear combination of the basis states. First labelling the sites in the Lieb SL according to their type (A, B, or C) and what unit cell they sit in ($n = 1, 2, \dots, N$), this prescription is as follows:

1. take antisymmetric (symmetric) combinations of the $|A_n\rangle$ and $|B_n\rangle$ basis states in the well (barrier) regions, then combine these symmetrically;
2. antisymmetrically combine every consecutive $|C_n\rangle$ site state throughout the superlattice;
3. the first (second) components in the new basis are then antisymmetric (symmetric) combinations of the two above results;
4. the remaining states are chosen to be other, orthogonal combinations of the basis states that numerically evaluate to (approximately) zero to maintain orthonormality.

To demonstrate this we choose the simplest case of $L = 2a$. Following the procedure outlined above, the wave function written in the new basis is

$$|\tilde{\psi}\rangle = U|\psi\rangle = \begin{bmatrix} (|A_1\rangle - |B_1\rangle + |A_2\rangle + |B_2\rangle)/2\sqrt{2} + (|C_1\rangle - |C_2\rangle)/2 \\ (|A_1\rangle - |B_1\rangle + |A_2\rangle + |B_2\rangle)/2\sqrt{2} - (|C_1\rangle - |C_2\rangle)/2 \\ (|A_1\rangle - |B_1\rangle - |A_2\rangle - |B_2\rangle)/2 \\ (|A_1\rangle + |B_1\rangle)/\sqrt{2} \\ (|A_2\rangle - |B_2\rangle)/\sqrt{2} \\ (|C_1\rangle + |C_2\rangle)/\sqrt{2} \end{bmatrix}. \quad (\text{S.2})$$

Then, performing the corresponding unitary transformation on the original $L = 2a$ Lieb SL Hamiltonian H gives the 2×2 block

$$H_0 = \begin{bmatrix} 0 & i\sqrt{2}\sin(k_x a/2) \\ -i\sqrt{2}\sin(k_x a/2) & 0 \end{bmatrix}, \quad (\text{S.3})$$

which has the required two zero-eigenvalues at the location of the ADC crossing.

S2 Continuum model calculation

The low energy and long wavelength continuum model calculation of the electronic states of the Lieb lattice under a 1D periodic can be done using the Transfer Matrix (TM) formalism. The eigenstates of the pristine system at low energies near the \mathbf{M} point (see Fig. 1(b)) are

$$\psi_\alpha(\mathbf{r}, \mathbf{k}) = \begin{bmatrix} \sin \phi_{\mathbf{k}} \\ \alpha \\ \cos \phi_{\mathbf{k}} \end{bmatrix} e^{i\mathbf{k}\cdot\mathbf{r}}, \quad (\text{S.4})$$

where α is the band index (+1 for the conduction band, 0 for the flat band, -1 for valence band), \mathbf{k} is measured from \mathbf{M} , and the propagation direction $\phi_{\mathbf{k}} = \tan^{-1}(k_y/k_x)$. Translational invariance along y means the problem reduces to 1D. These are matched at the well-barrier interface using the matching conditions

$$\psi_B^+(x) = \psi_B^-(x), \quad \psi_C^+(x) = \psi_C^-(x), \quad (\text{S.5})$$

in order to build the TM T . The + (−) correspond to states approaching the well-barrier interface from the left (right). The TM is built using a product of the Wronskians \mathcal{W} of the matched eigenstates at the well-barrier interfaces, given by

$$T = \mathcal{W}_{k_x,b}(L)\mathcal{W}_{k_x,b}^{-1}(W)\mathcal{W}_{k_x,w}(W)\mathcal{W}_{k_x,w}^{-1}(0). \quad (\text{S.6})$$

Here, $k_{x,w} = \sqrt{(\frac{E}{\hbar v_F})^2 - k_y^2}$ and $k_{x,b} = \sqrt{(\frac{E-V_0}{\hbar v_F})^2 - k_y^2}$ are the x -components of \mathbf{k} in the well and barrier regions. $\hbar v_F$ is the Fermi velocity of the Dirac bands. Explicitly, at a position x , we have

$$\mathcal{W}_k(x) = \begin{bmatrix} \alpha e^{ikx} & \alpha e^{-ikx} \\ \cos(\phi_{\mathbf{k}})e^{ikx} & -\cos(\phi_{\mathbf{k}})e^{-ikx} \end{bmatrix}. \quad (\text{S.7})$$

The fact that $\text{Tr}(T) = 2\cos(k_x L)$, with k_x the superlattice wave vector along x , gives the dispersion relation

$$\begin{aligned} \cos(k_x L) &= \cos(k_{x,w}W)\cos(k_{x,b}W) \\ &\quad - \frac{1}{2}\sin(k_{x,w}W)\sin(k_{x,b}W)\left(\frac{\cos\phi}{\cos\theta} + \frac{\cos\theta}{\cos\phi}\right), \end{aligned} \quad (\text{S.8})$$

where ϕ and θ are the propagation directions in the well and barrier respectively.

S3 Supplementary figures

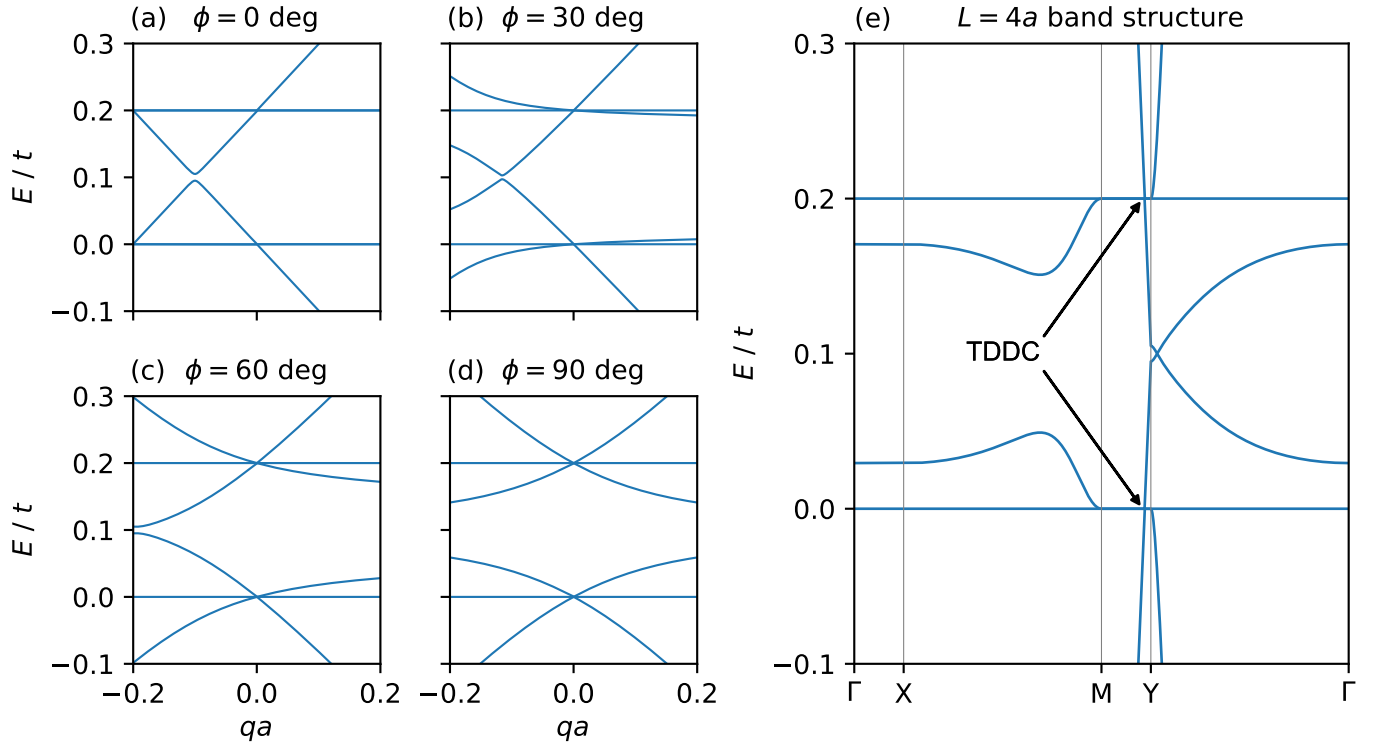


Fig. S1. Band structure around the triply degenerate Dirac cone (TDDC). (a-d) The band structures along small reciprocal space distances q measured from the TDDC. In each subplot the angle of this cut is rotated by ϕ ($\phi = 0$ defined as along $\mathbf{Y} \rightarrow \mathbf{M}$). (e) The low-energy $L = 4a$ Lieb SL band structure with TDDCs indicated.

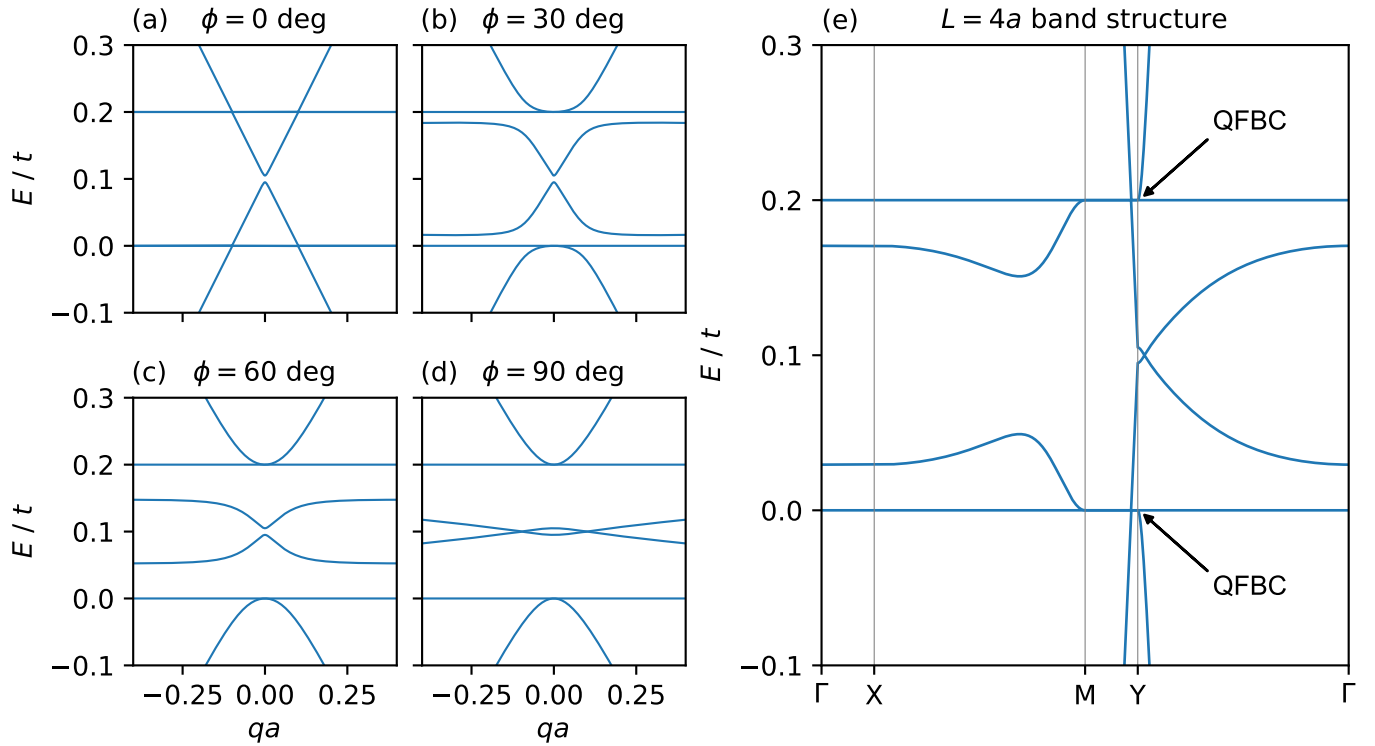


Fig. S2. Band structure around the Y point. (a-d) The band structures along small reciprocal space distances q measured from the Y point at $\mathbf{k} = (0, \pi)$. In each subplot the angle of this cut is rotated by ϕ ($\phi = 0$ defined as along $\mathbf{Y} \rightarrow \mathbf{M}$). (e) The low-energy $L = 4a$ Lieb SL band structure with QFBCs indicated.

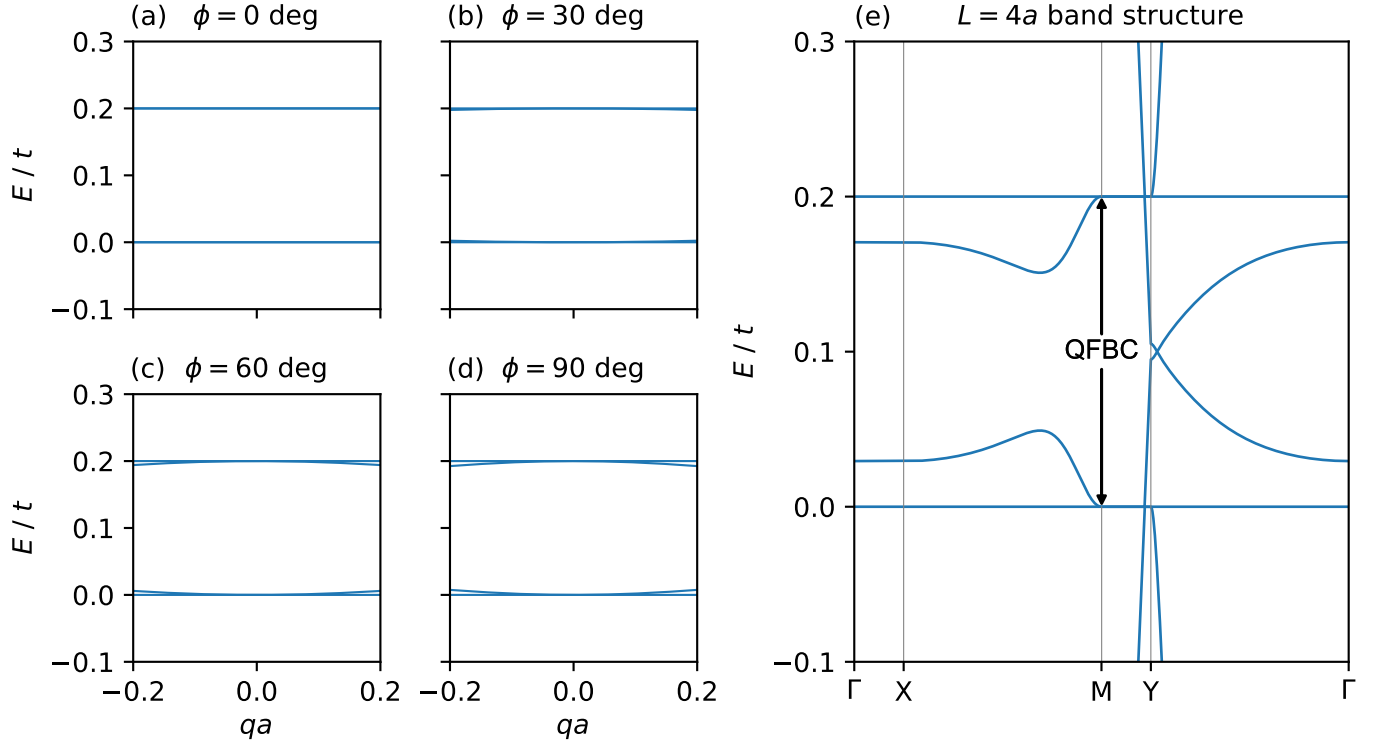


Fig. S3. Band structure around the M point. (a-d) The band structures along small reciprocal space distances q measured from the **M** point at $\mathbf{k} = (\pi/L, \pi)$. In each subplot the angle of this cut is rotated by ϕ ($\phi = 0$ defined as along $\mathbf{Y} \rightarrow \mathbf{M}$). (e) The low-energy $L = 4a$ Lieb SL band structure with QFBCs indicated.

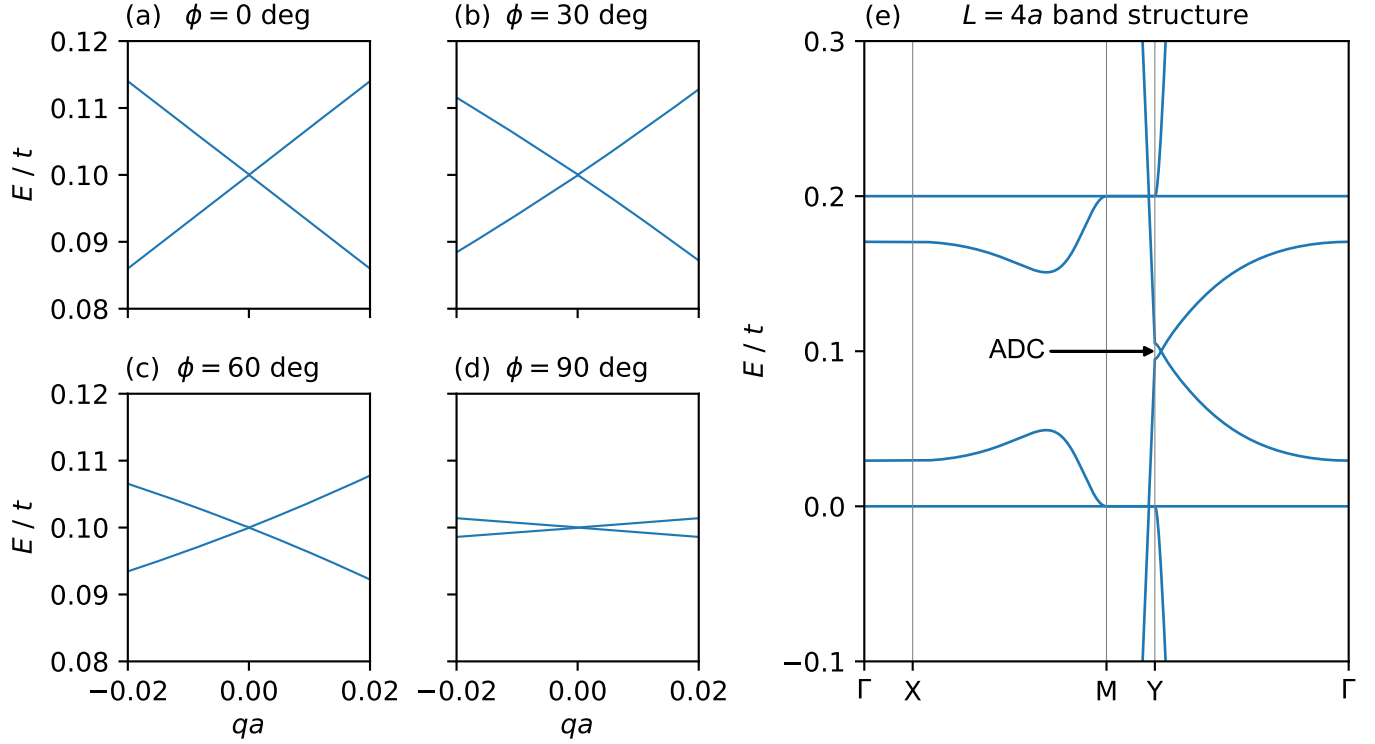


Fig. S4. Band structure around the anisotropic Dirac cone (ADC). (a-d) The band structures along small reciprocal space distances q measured from the ADC crossing point at $\mathbf{k} = (0, \pi - V_0/2)$. In each subplot the angle of this cut is rotated by ϕ ($\phi = 0$ defined as along $\mathbf{Y} \rightarrow \mathbf{M}$). (e) The low-energy $L = 4a$ Lieb SL band structure with ADC indicated.

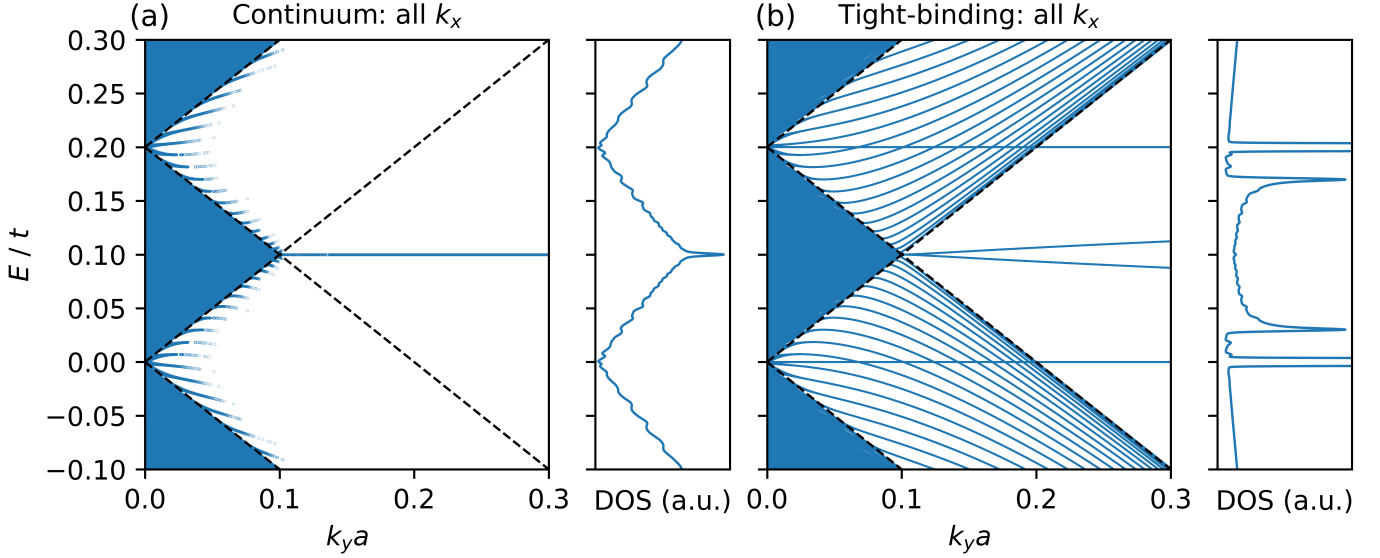


Fig. S5. Continuum vs Tight-Binding comparison for states near the Y point. The region of the Brillouin Zone as in Fig. 2(a-b) but allowing for all k_x values ($0 < k_x < \pi/L$). For the continuum model description in (a), this amounts to allowing all solutions for the derived dispersion relation in Eq. S.8. In (b), we superpose the calculated bands for 20 values of k_x in the range ($0 < k_x < \pi/L$).

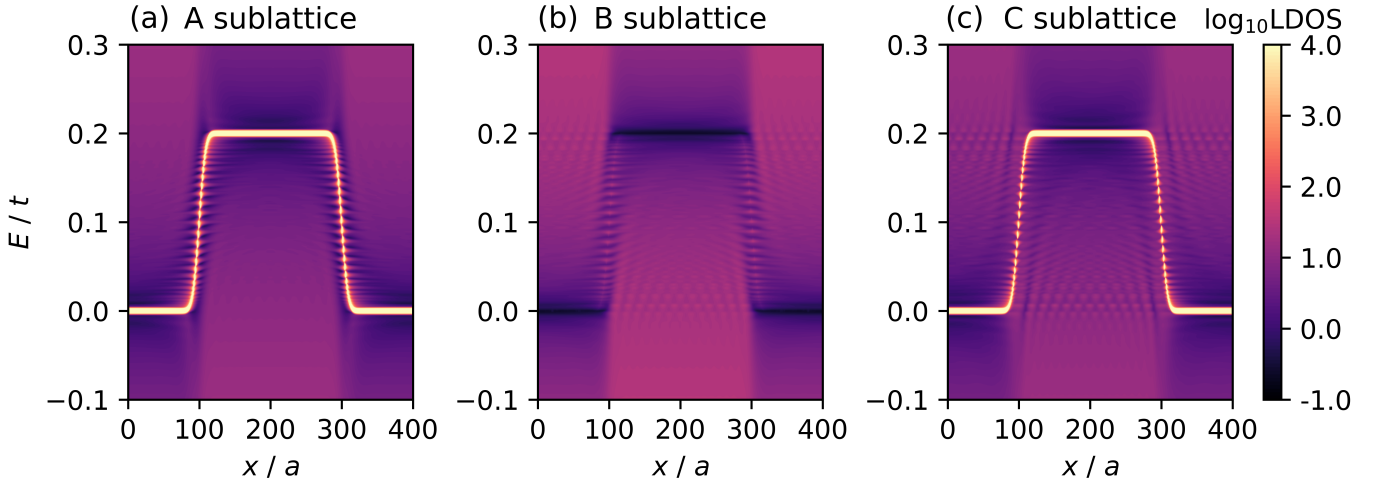


Fig. S6. LDOS spectra for A, B and C sublattices under a smoothed potential. The potential parameters are $L = 400a$, $V_0 = 0.2t$, as used in the main text in Fig. 5. The smoothness parameter $\alpha = 10^{-2}$.

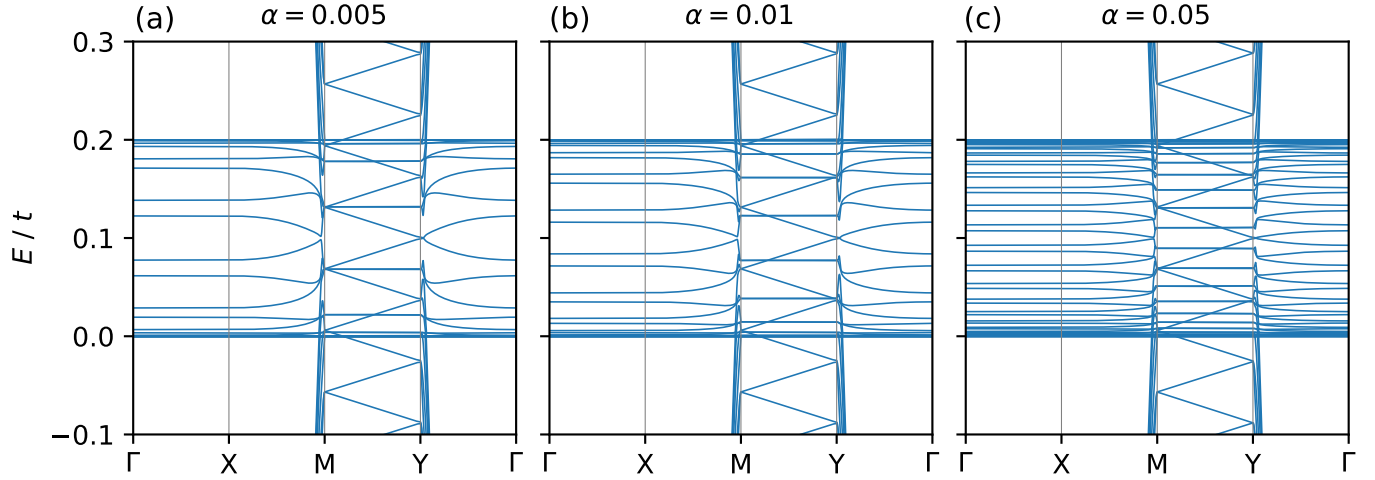


Fig. S7. Full band structures of Lieb SL for different potential smoothness. The potential parameters are $L = 100a$, $V_0 = 0.2t$. The smoothness parameters are (a) $\alpha = 0.005$, (b) $\alpha = 0.01$, (c) $\alpha = 0.05$. The reciprocal space distances $|\Gamma\mathbf{X}|$ and $|\mathbf{M}\mathbf{Y}|$ are kept artificially constant for visualisation purposes. These distances are $|\Gamma\mathbf{X}| = |\mathbf{M}\mathbf{Y}| = |\mathbf{Y}\Gamma|/N$ due to folding of the BZ. Each pair of discrete lattice symmetry broken states generate two additional partial flat bands along $\Gamma\mathbf{X}$ and a doubly degenerate flat band along $\mathbf{M}\mathbf{Y}$.

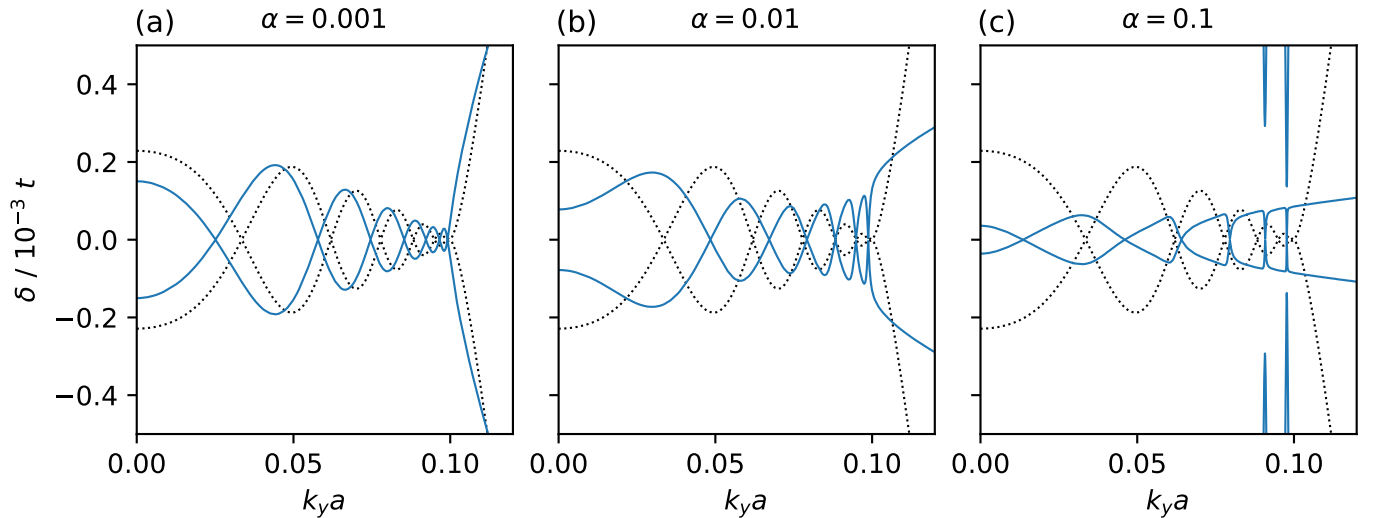


Fig. S8. The braided bands at $E = V_0/2$ for different SL potential smoothness. States plotted along k_y with k_y measured from \mathbf{Y} (as in main text). The potential parameters are $L = 400a$, $V_0 = 0.2t$, as used in the main text in Fig. 5. The smoothness parameters values used are (a) $\alpha = 0.001$, (b) $\alpha = 0.01$, (c) $\alpha = 0.1$.

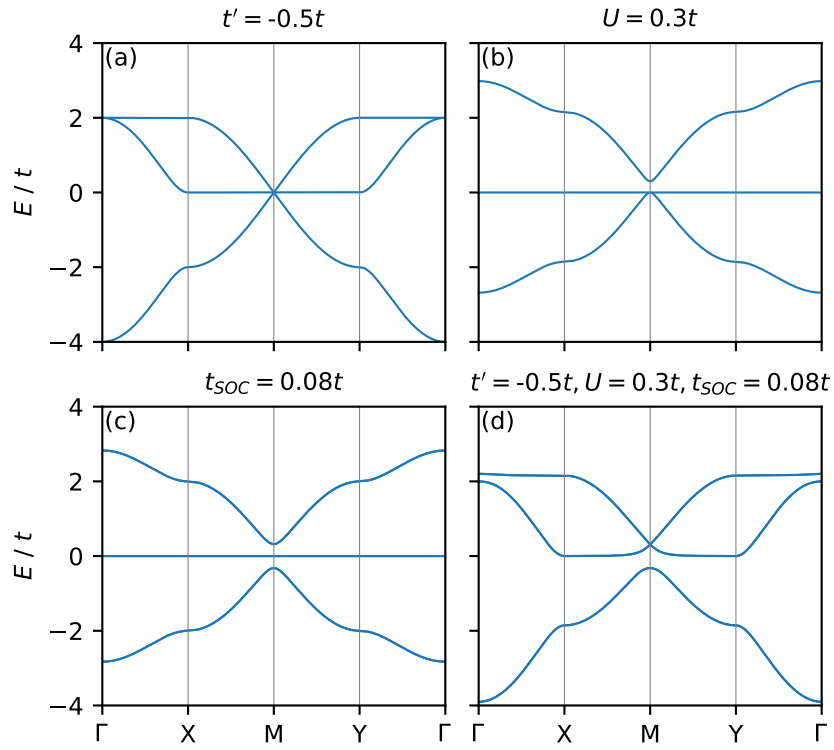


Fig. S9. Adding additional parameters to the pristine Lieb lattice. Pristine Lieb lattice (absence of periodic potential) band structures upon inclusion of (a) a next-nearest neighbour interaction, (b) a mass term, (c) spin-orbit coupling, and (d) all of the above. The values used are shown in the respective panels. High symmetry points of the pristine Lieb lattice are $\Gamma(0,0)$, $\mathbf{X}(\frac{\pi}{a},0)$, $\mathbf{M}(\frac{\pi}{a},\frac{\pi}{a})$, $\mathbf{Y}(0,\frac{\pi}{a})$.

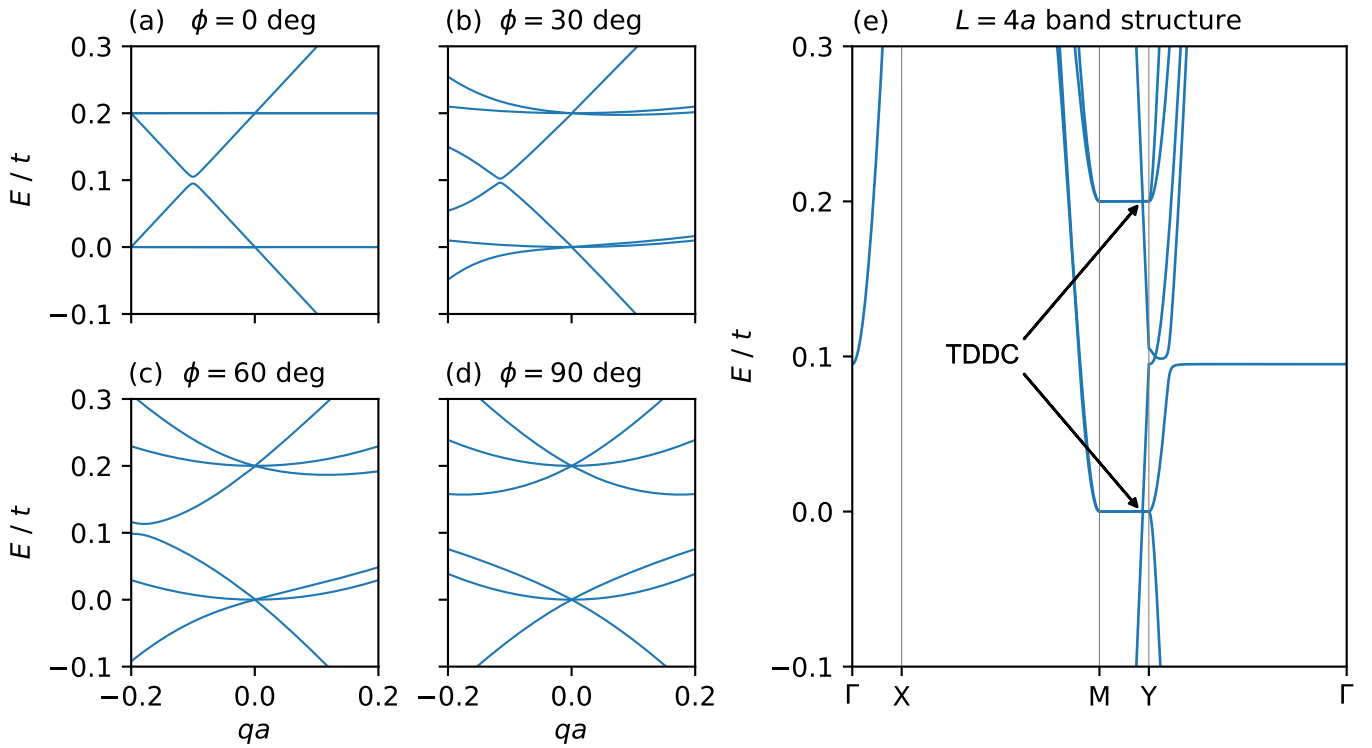


Fig. S10. Band structure around the TDDC with NNN hoppings. The same as Figure S1 but with a NNN hopping term $t' = -0.5t$. The flat band disperses for all directions except for $\phi = 0$ (along $\mathbf{Y} \rightarrow \mathbf{M}$).

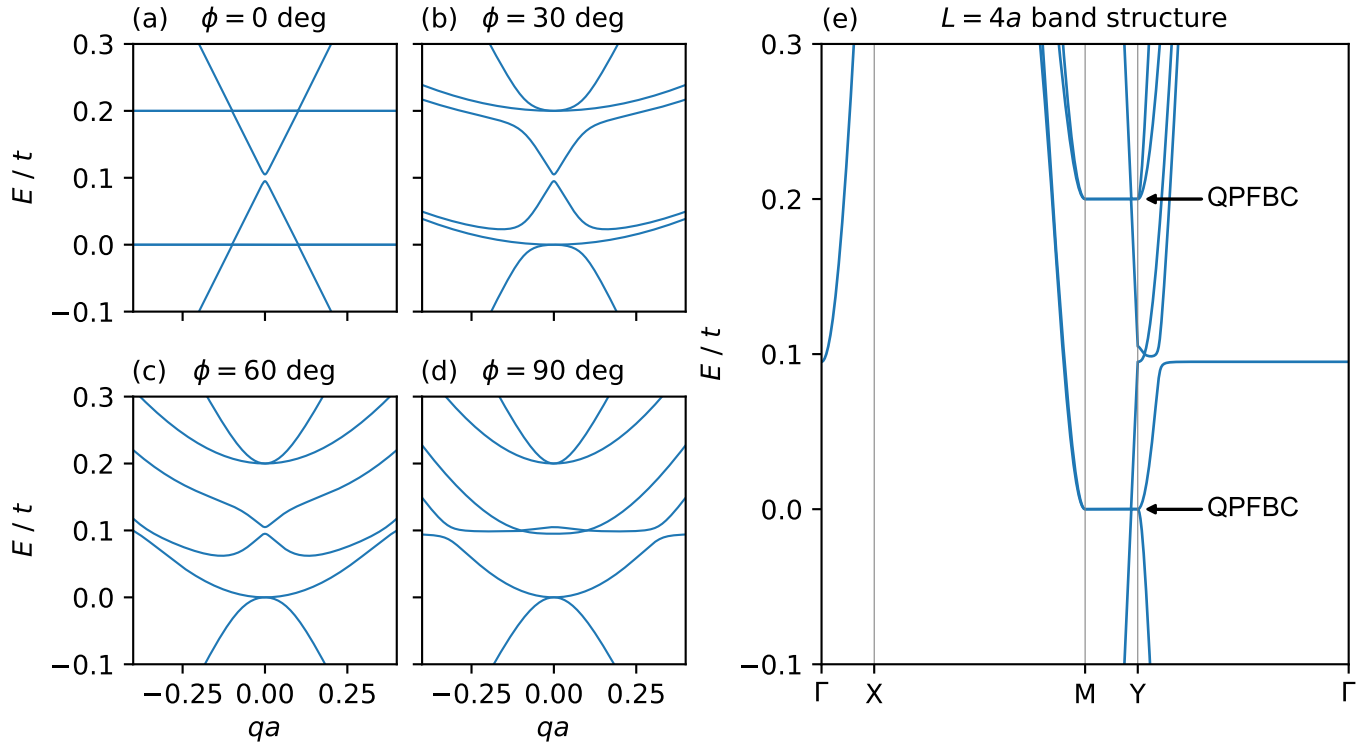


Fig. S11. Band structure around the Y point with NNN hoppings. The same as Figure S2 but with a NNN hopping term $t' = -0.5t$. The dispersing flat band turns the quadratic flat band crossings (QFBCs) into quadratic band crossings (QBCs) with curvatures of opposite (same) sign at $E = 0$ (V_0).

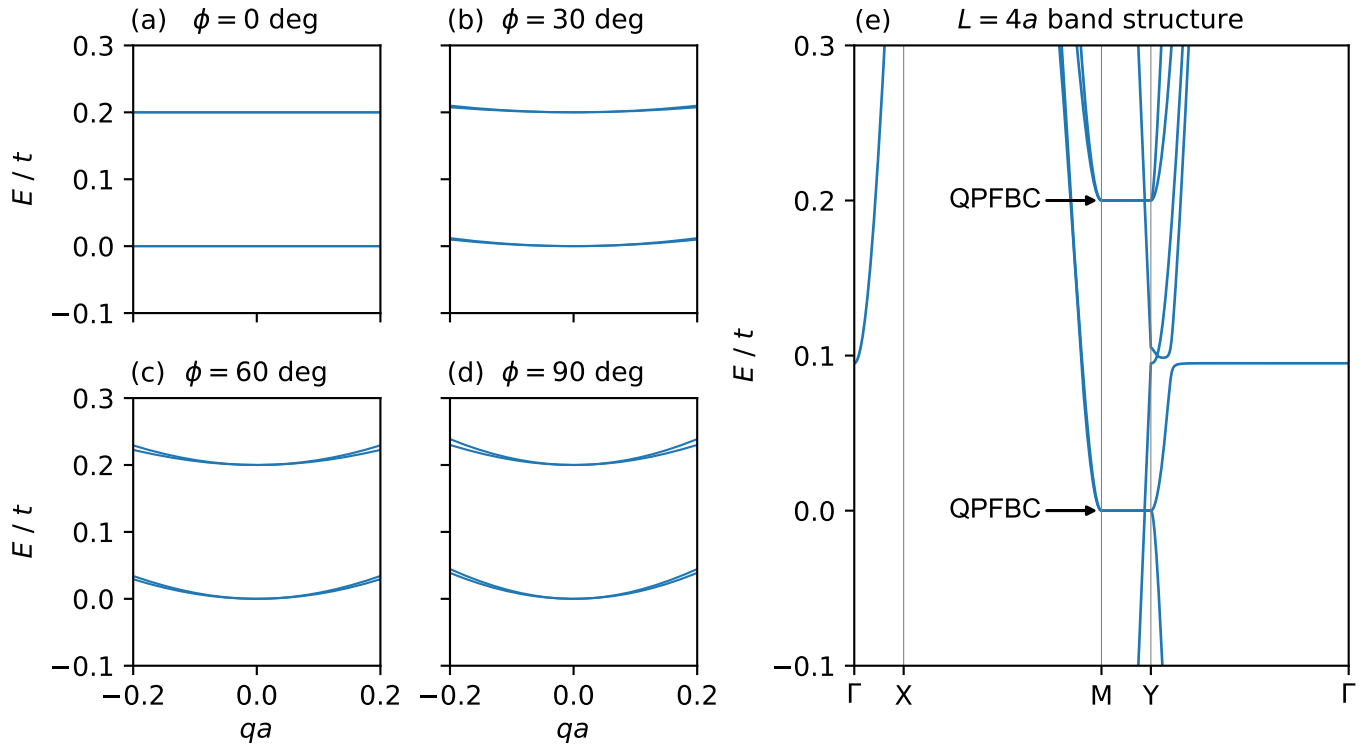


Fig. S12. Band structure around the M point with NNN hoppings. The same as Figure S3 but with a NNN hopping term $t' = -0.5t$.

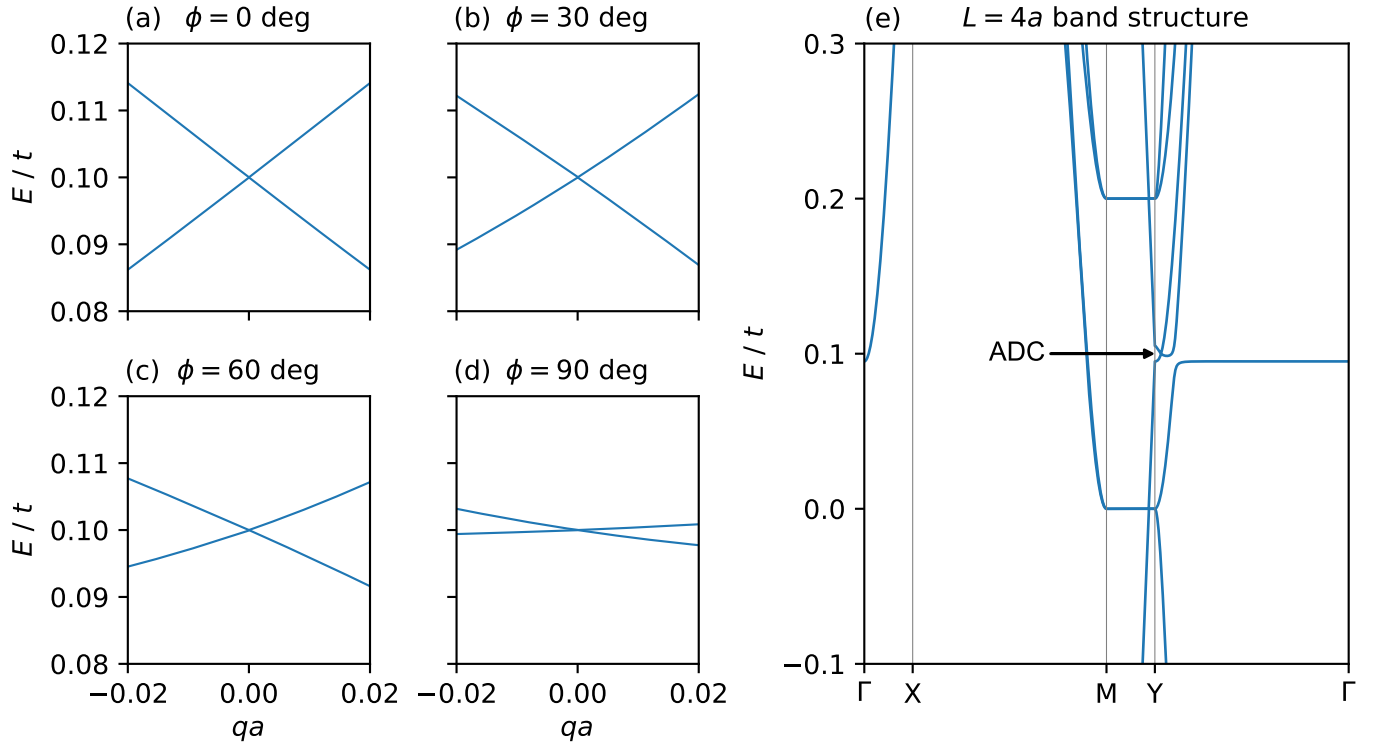


Fig. S13. Band structure around the ADC with NNN hoppings. The same as Figure S4 but with a NNN hopping term $t' = -0.5t$.

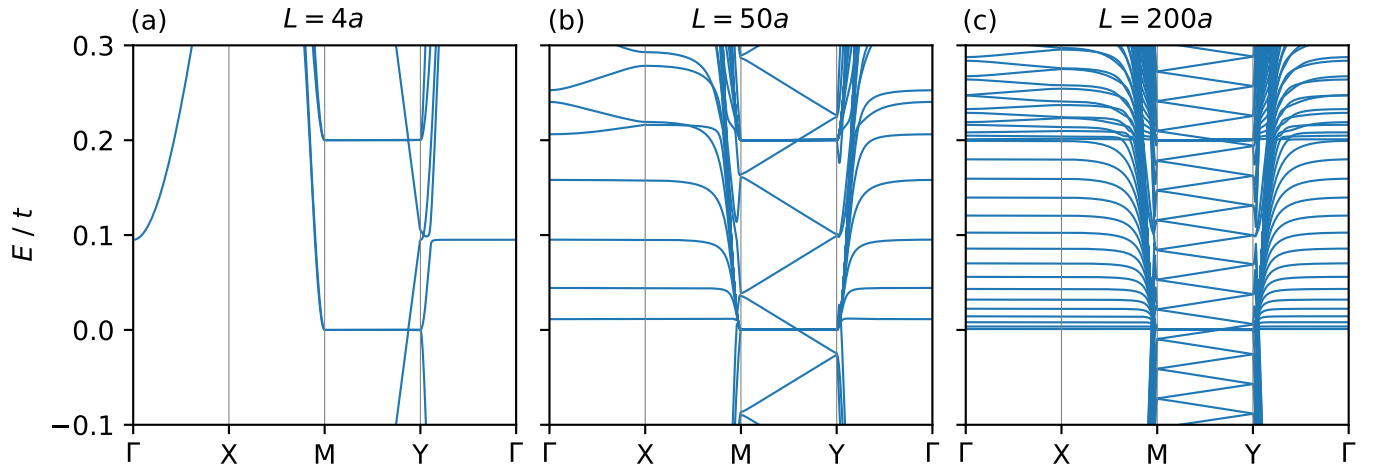


Fig. S14. Lieb SL band structure with next-nearest neighbour (NNN) hoppings. Band structures along high-symmetry directions for SL periodicities (a) $L = 4a$, (b) $L = 50a$, and (c) $L = 200a$ with a NNN hopping parameter $t' = -0.5t$. The reciprocal space distances ΓX and MY are kept artificially constant to visualise the band folding MY which remains unchanged from the nearest-neighbour only case.

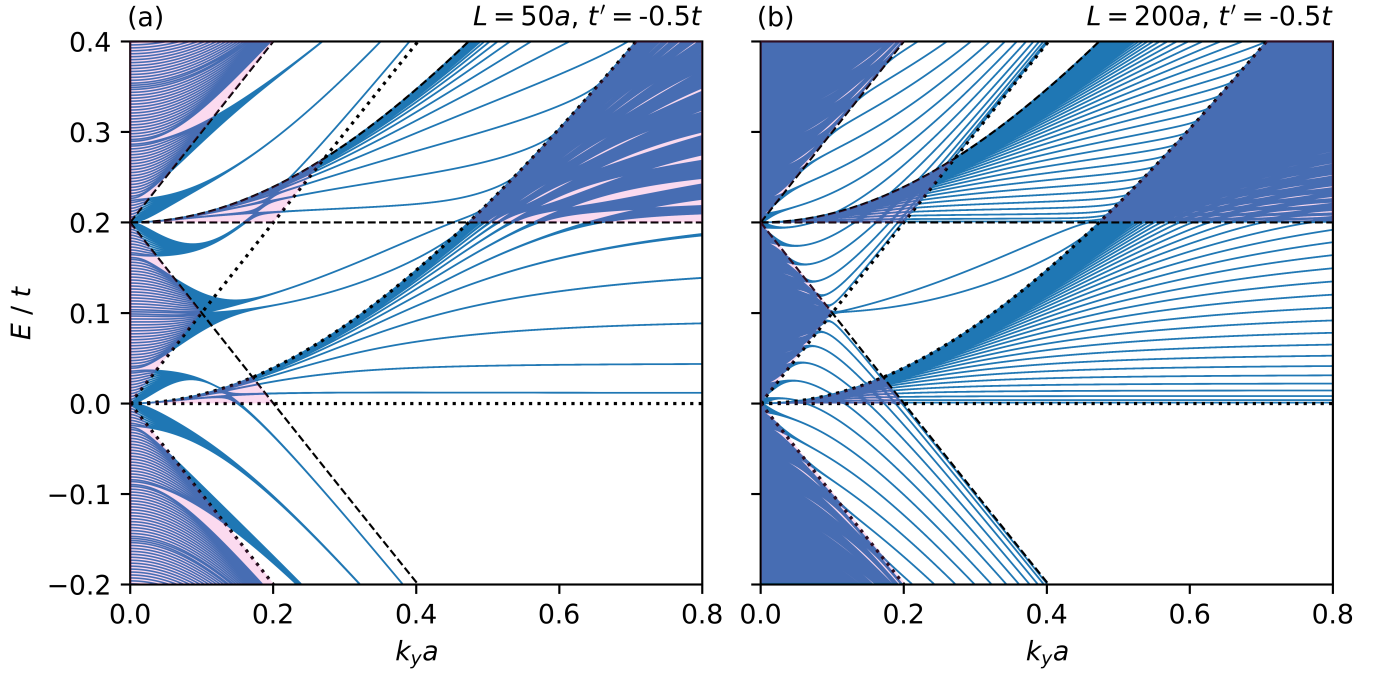


Fig. S15. Bands near the Y point for multiple k_x values with next-nearest neighbours (NNN). Bands near the Y point plotted for 20 k_x values in the range $k_x : [0, \pi/L]$ with NNN hopping parameter $t' = -0.5t$ and SL periodicities (a) $L = 50a$, and (b) $L = 200a$. The shaded pink regions show where electronic states are allowed in both well and barrier regions according to their respective pristine dispersions.

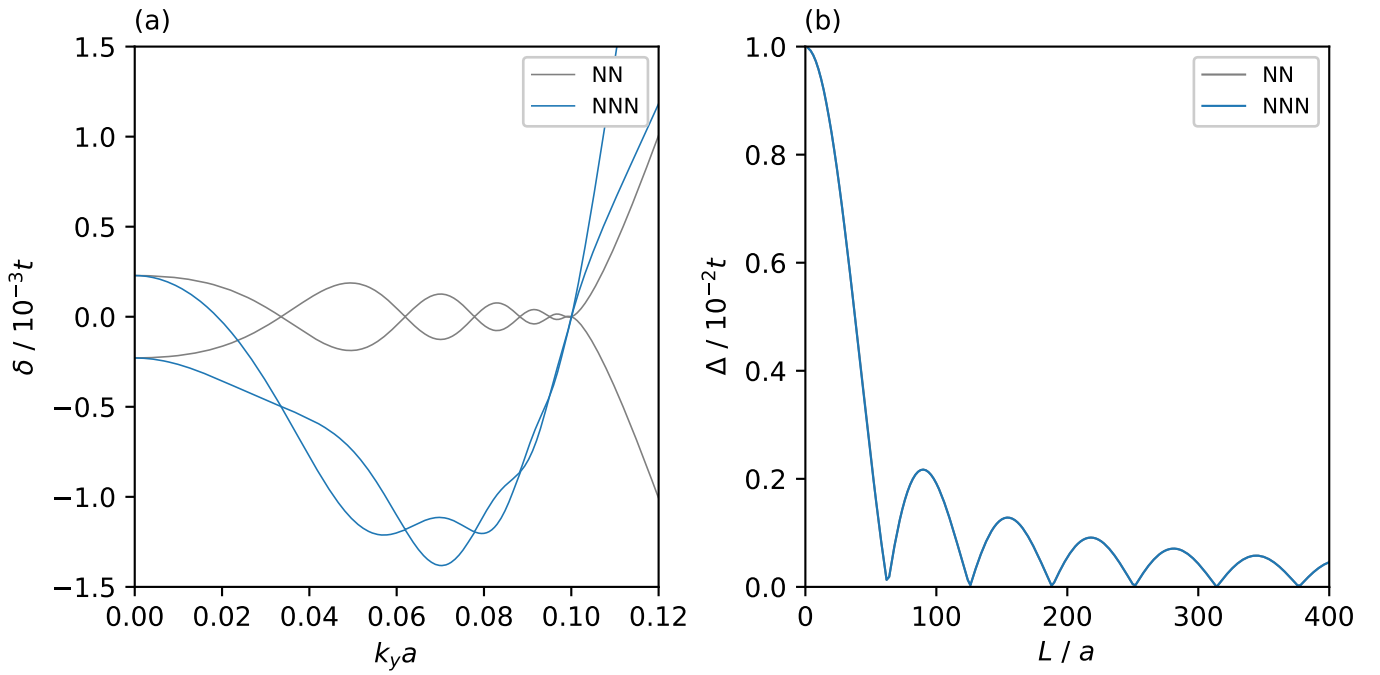


Fig. S16. States near $E = V_0/2$ with NNN. (a) Inclusion of NNN (blue curve) shifts the energies of additional crossings generated at large SL periodicities compared to the NN only case (grey curve) (b) However, since the band folding along **MY** remains unchanged, the number and location of additional cones is identical to that of the NN case (the blue and grey curve are overlaid).

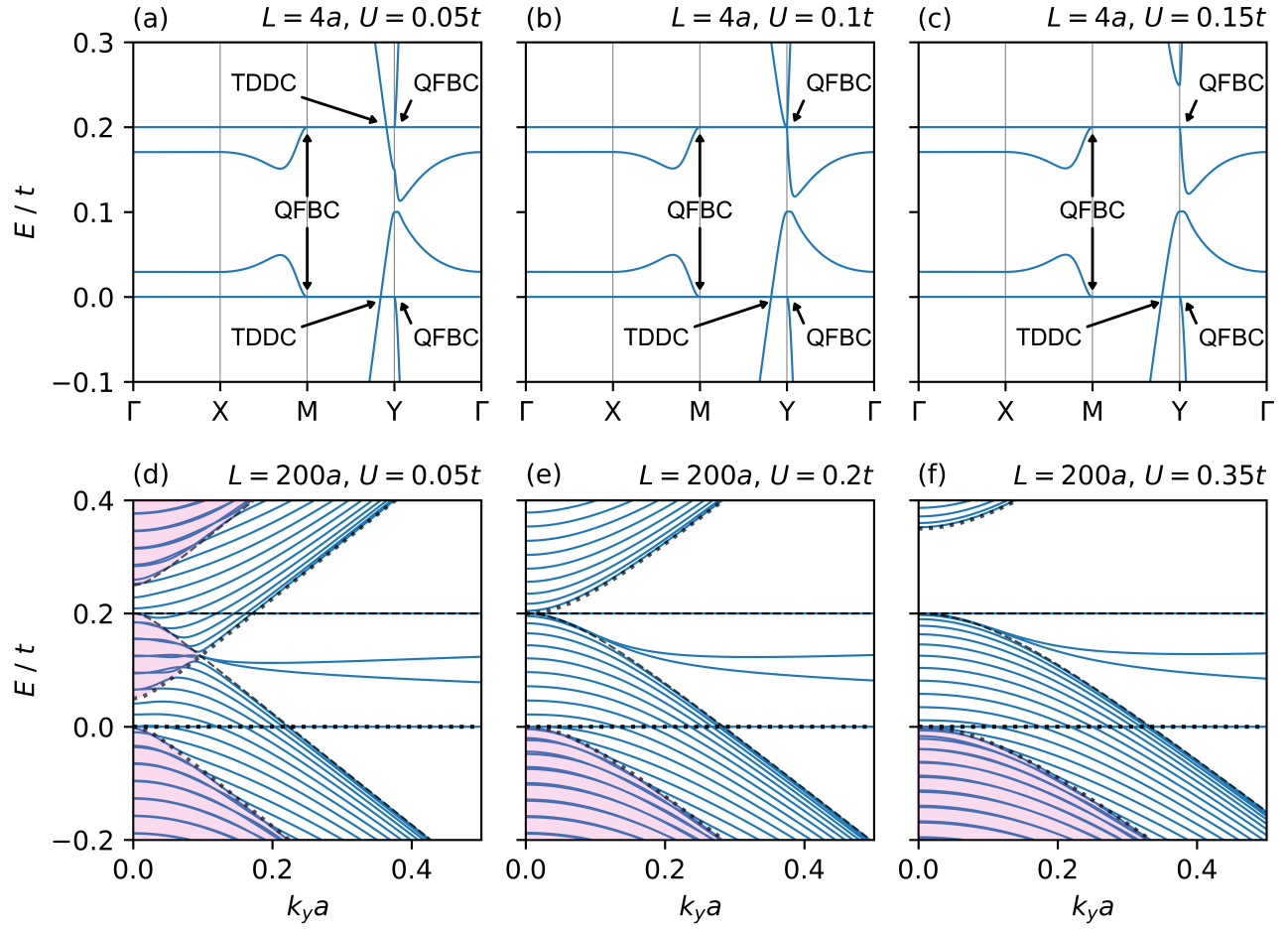


Fig. S17. Evolution of the SL dispersion and opening of a band gap with the inclusion of a mass term. Potential height is $V_0 = 0.2t$ in all plots. In the discrete limit (top row, $L = 4a$), a mass term $|U| > V_0/2$ is required to open a band gap. In the continuum limit (bottom row, $L = 200a$), a mass term $|U| > V_0$ is needed. Only positive values of U are shown, where the gap opens above the flat band at $E = V_0$. For $U < 0$ the gap appears below the flat band at $E = 0$. The shaded pink regions show where electronic states are allowed in both well and barrier regions according to their respective pristine dispersions.

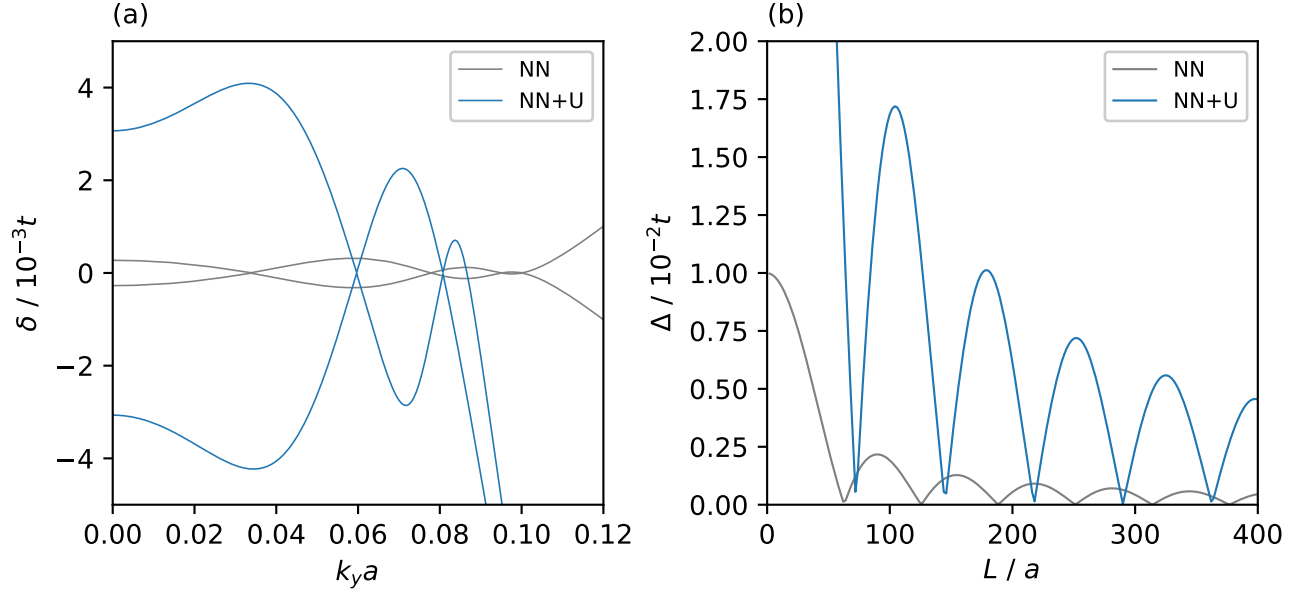


Fig. S18. States near the SKT energies with a mass term. The SL height is $V_0 = 0.2t$. (a) Fewer additional anisotropic cones are generated at the “SKT” energies: $E = V_0/2$ for the NN only case, and $E = (V_0 + U)/2$ when mass term is included. Here, the SL periodicity is $L = 200a$. (b) For a given V_0 , a larger periodicity L is required to close the gap at \mathbf{Y} and generate the additional ADCs, hence fewer ADCs form in the presence of a mass term.

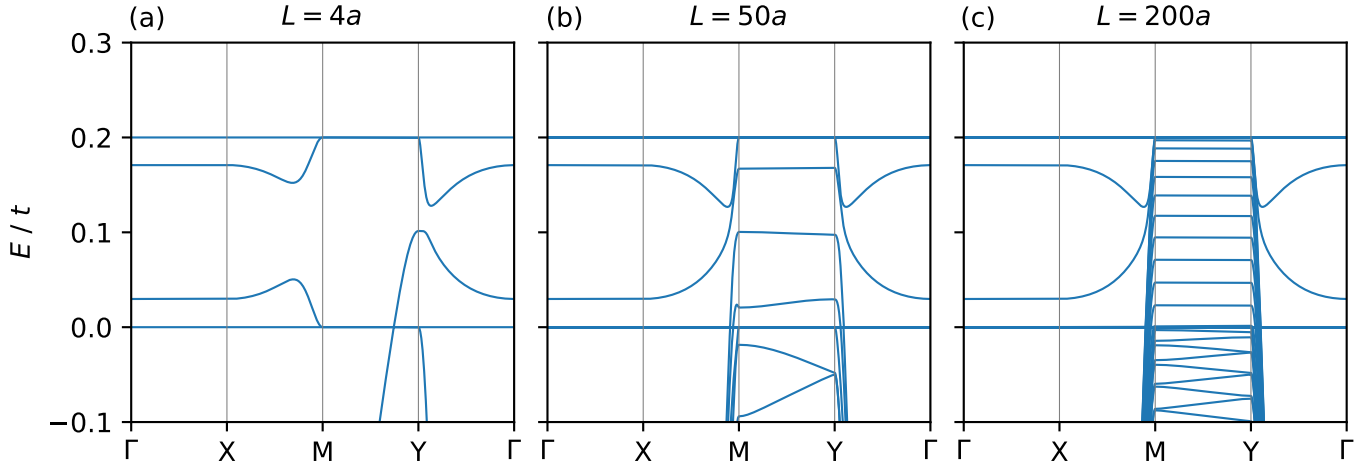


Fig. S19. Lieb SL band structure with an effective mass term. Band structures along high-symmetry directions for SL periodicities (a) $L = 4a$, (b) $L = 50a$, and (c) $L = 200a$ for a mass term $U = 0.3t$. The reciprocal space distances ΓX and MY are kept artificially constant to visualise the band folding MY .

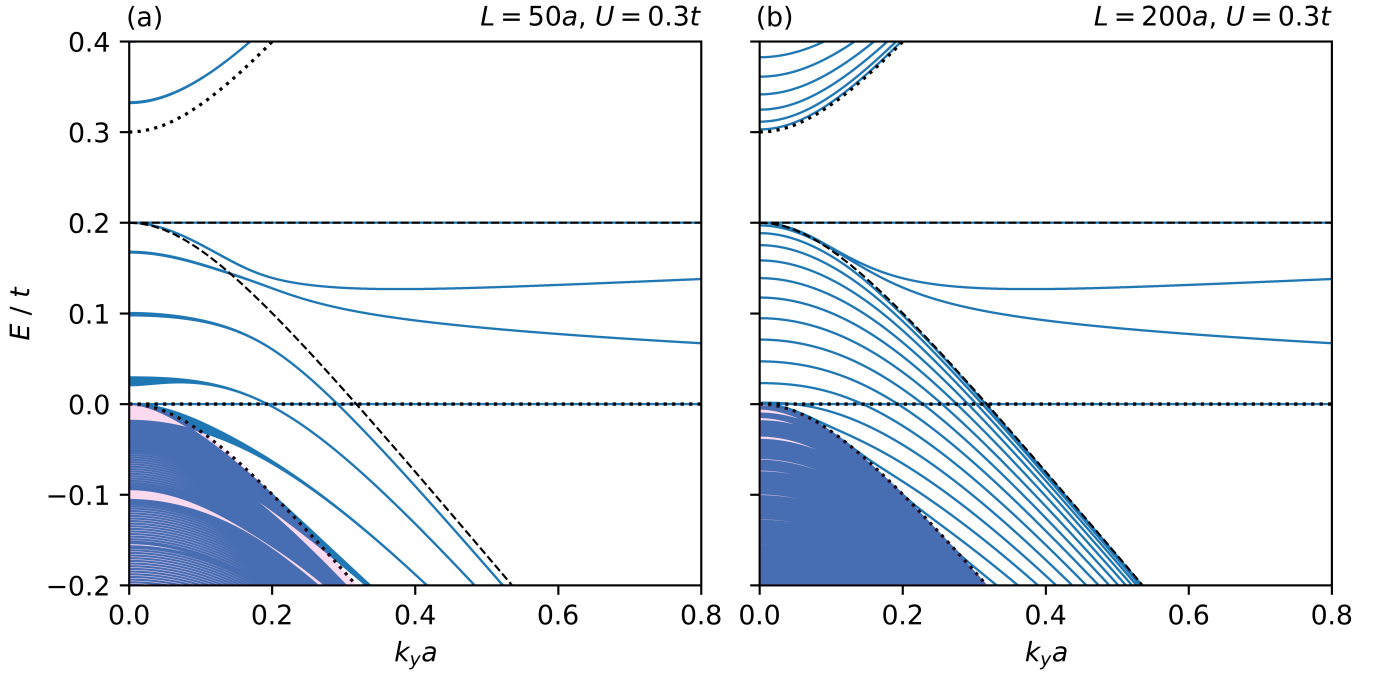


Fig. S20. Bands near the Y point for multiple k_x values with an effective mass term. Bands near the Y point plotted for 20 k_x values in the range $k_x \in [0, \pi/L]$ with mass term $U = 0.3t$ and SL periodicities (a) $L = 50a$, and (b) $L = 200a$. The shaded pink regions show where electronic states are allowed in both well and barrier regions according to their respective pristine dispersions.

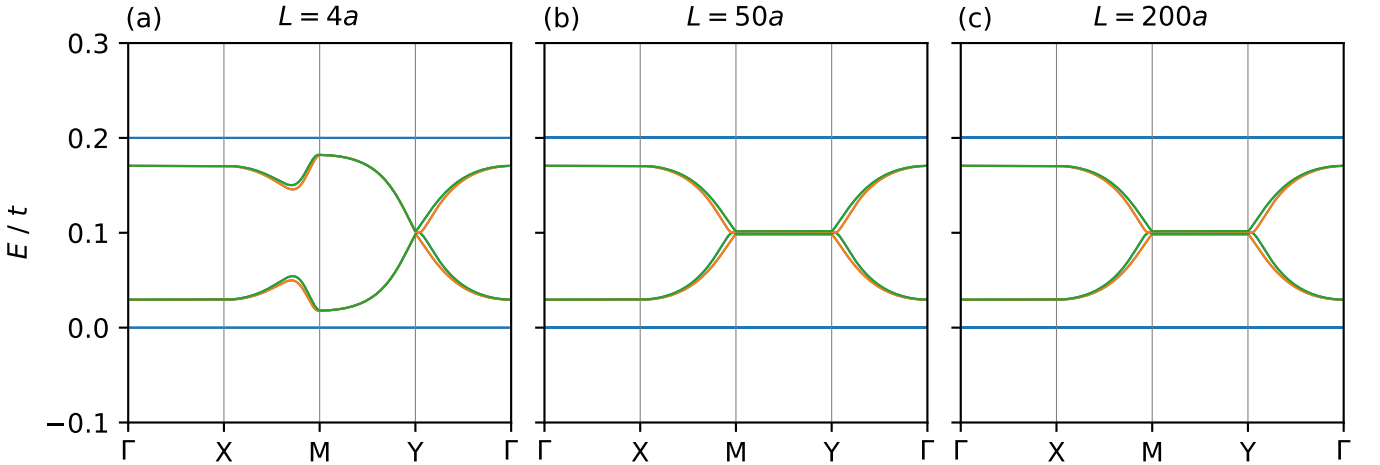


Fig. S21. Lieb SL band structure with spin-orbit coupling (SOC). Band structures along high-symmetry directions for SL periodicities (a) $L = 4a$, (b) $L = 50a$, and (c) $L = 200a$ with an SOC interaction $t_{\text{SOC}} = 0.08t$. The reciprocal space distances ΓX and MY are kept artificially constant to visualise the band folding MY . Green and orange bands indicate the spin-splitting of the interface states that arises from discrete lattice symmetry breaking at the well-barrier interface. This only occurs along XM and ΓY ; the spin-up and spin-down states are degenerate along ΓX and MY .

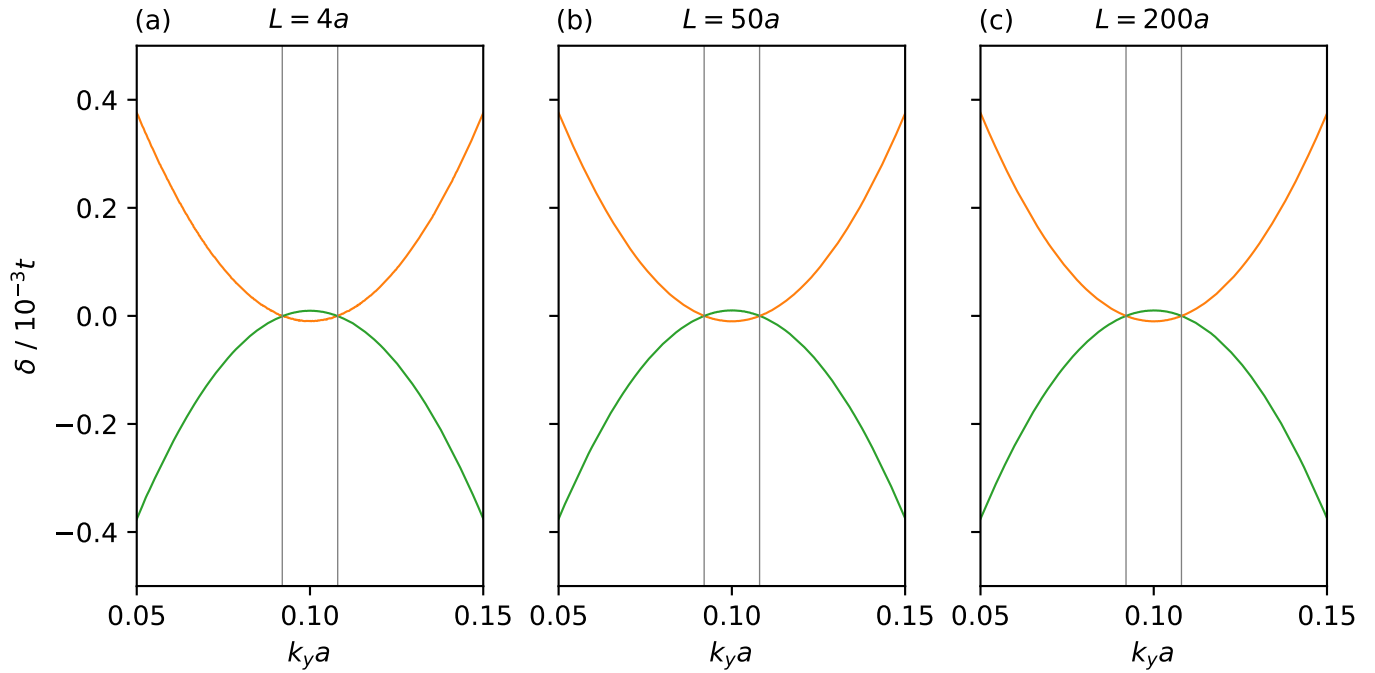


Fig. S22. States near $E = V_0/2$ with a spin-orbit coupling (SOC) term. For SL periodicities (a) $L = 4a$, (b) $L = 50a$, (c) $L = 200a$, the number and locations of the spin-polarised anisotropic cones remain unchanged, since the continuum states that would otherwise fold down to $E = V_0/2$ are prevented from doing so by the SOC term.

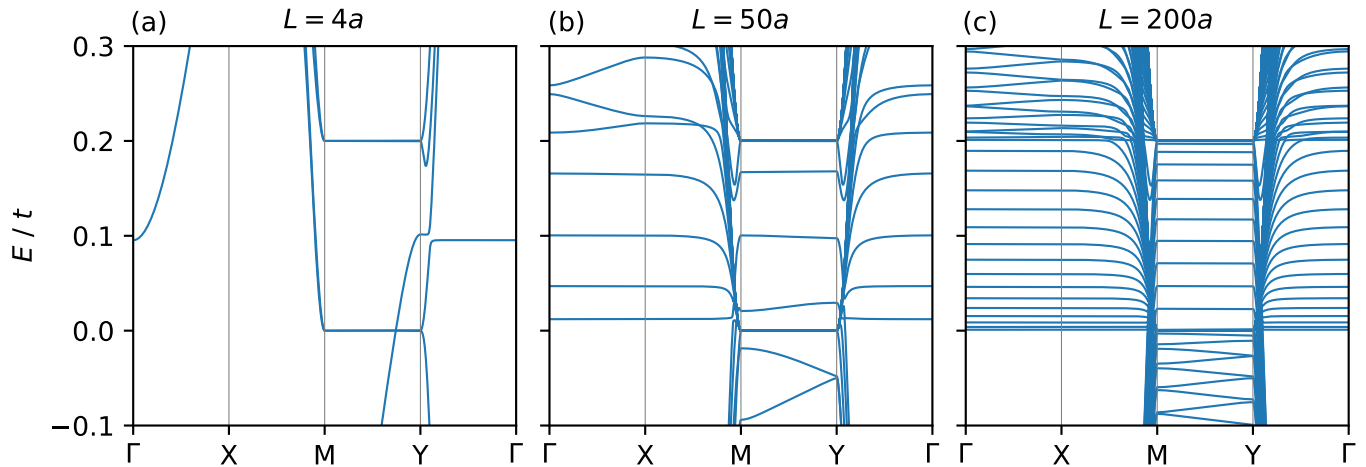


Fig. S23. Lieb SL band structure with next-nearest neighbour (NNN) hoppings and a mass term. Band structures along high-symmetry directions for SL periodicities (a) $L = 4a$, (b) $L = 50a$, and (c) $L = 200a$ with NNN hoppings $t' = -0.5t$ and mass term $U = 0.3t$. The reciprocal space distances ΓX and MY are kept artificially constant to visualise the band folding MY .

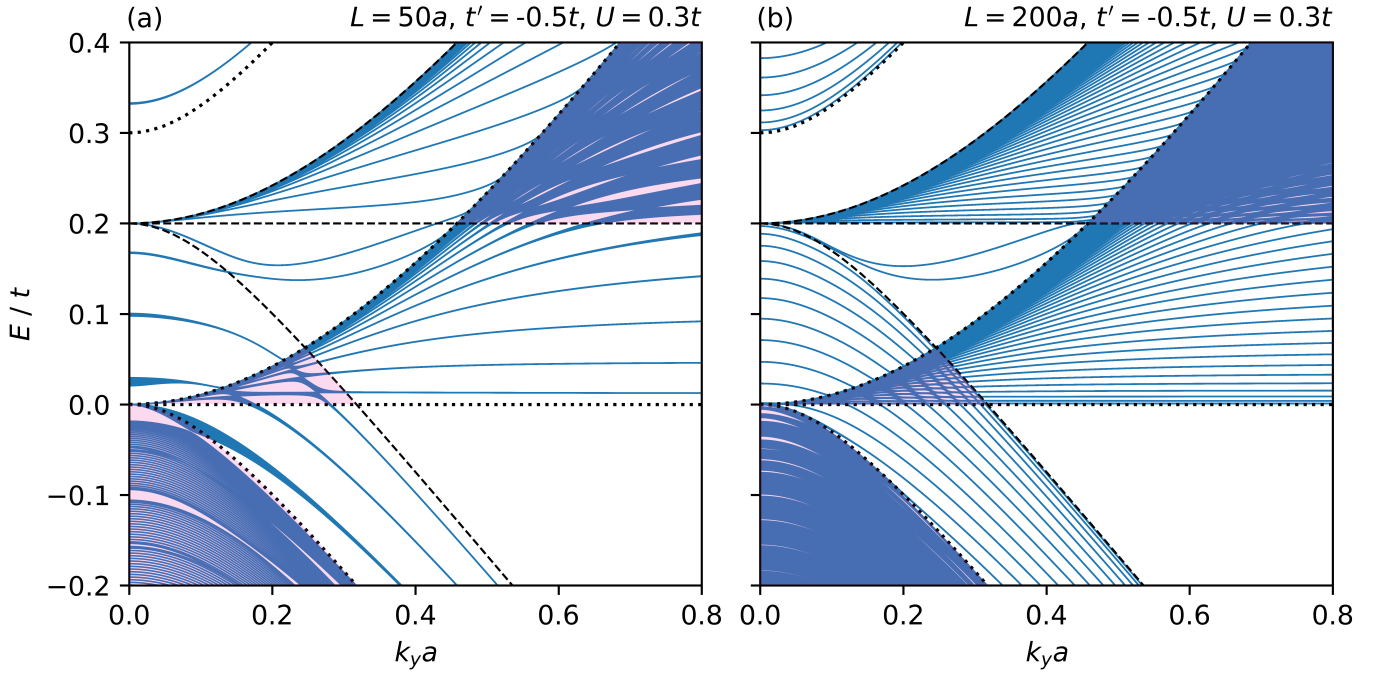


Fig. S24. Bands near the Y point for multiple k_x values with next-nearest neighbour hoppings and an effective mass term. Bands near the Y point plotted for 20 k_x values in the range $k_x : [0, \pi/L]$ for SL periodicities (a) $L = 50a$, and (b) $L = 200a$. The NNN hopping parameter $t' = -0.5t$ and mass term $U = 0.3t$. The shaded pink regions show where electronic states are allowed in both well and barrier regions according to their respective pristine dispersions.

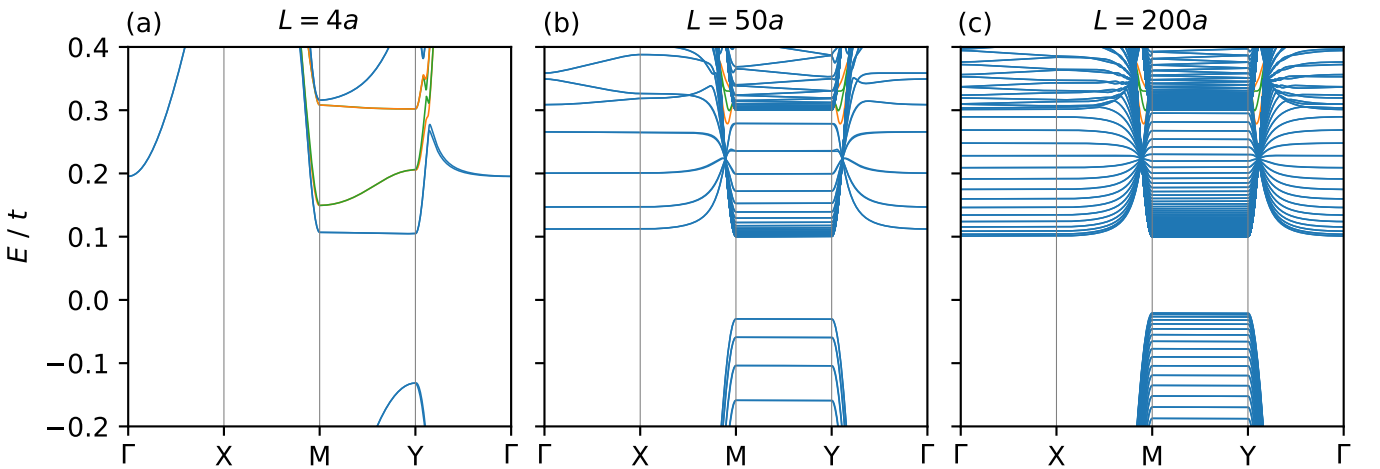


Fig. S25. Lieb SL band structure with all model parameters. Band structures along high-symmetry directions for SL periodicities (a) $L = 4a$, (b) $L = 50a$, and (c) $L = 200a$ with NNN hoppings $t' = -0.5t$, mass term $U = 0.3t$, and SOC interaction $t_{\text{SOC}} = 0.08t$. The reciprocal space distances ΓX and $M Y$ are kept artificially constant to visualise the band folding $M Y$.

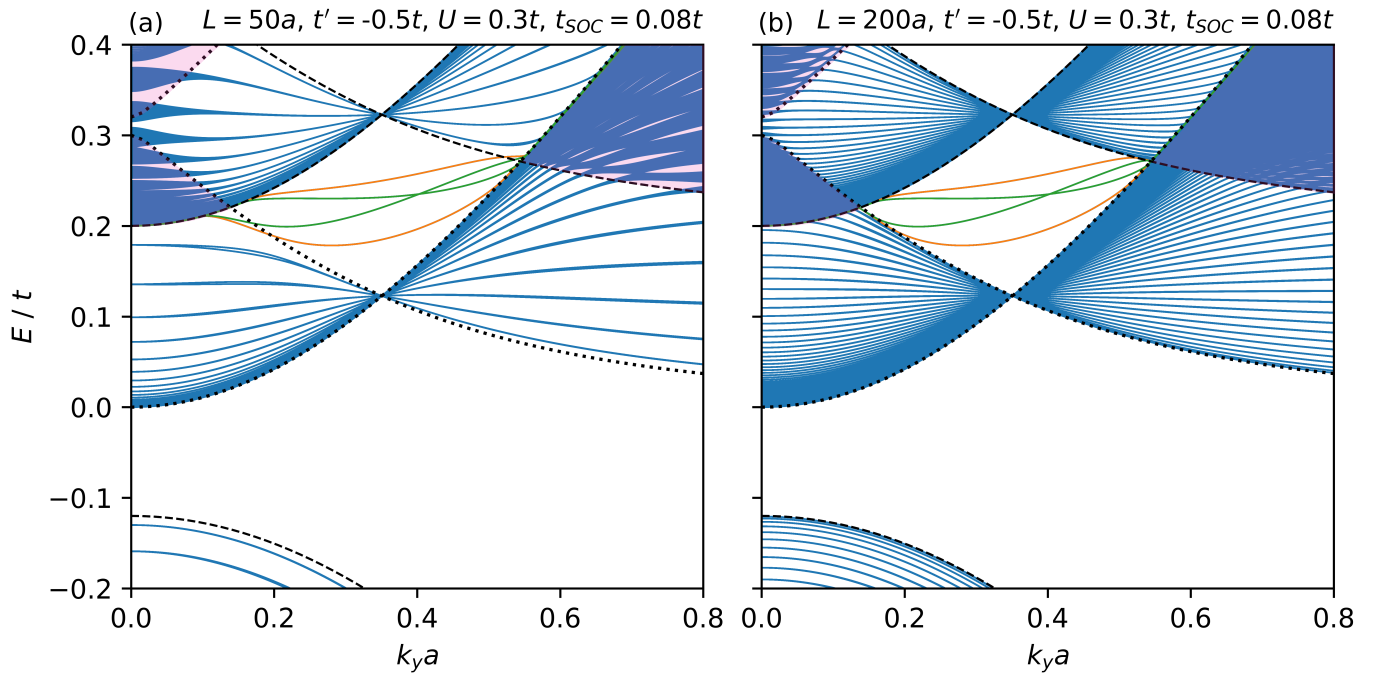


Fig. S26. Bands near the Y point for multiple k_x values with all model parameters: next-nearest neighbour (NNN) hoppings, an effective mass term, and spin-orbit coupling (SOC). Bands near the Y point plotted for 20 k_x values in the range $k_x : [0, \pi/L]$ for SL periodicities (a) $L = 50a$, and (b) $L = 200a$. The NNN hopping parameter $t' = -0.5t$, the mass term $U = 0.3t$, and the SOC strength $t_{SOC} = 0.08t$. The shaded pink regions show where electronic states are allowed in both well and barrier regions according to their respective pristine dispersions.

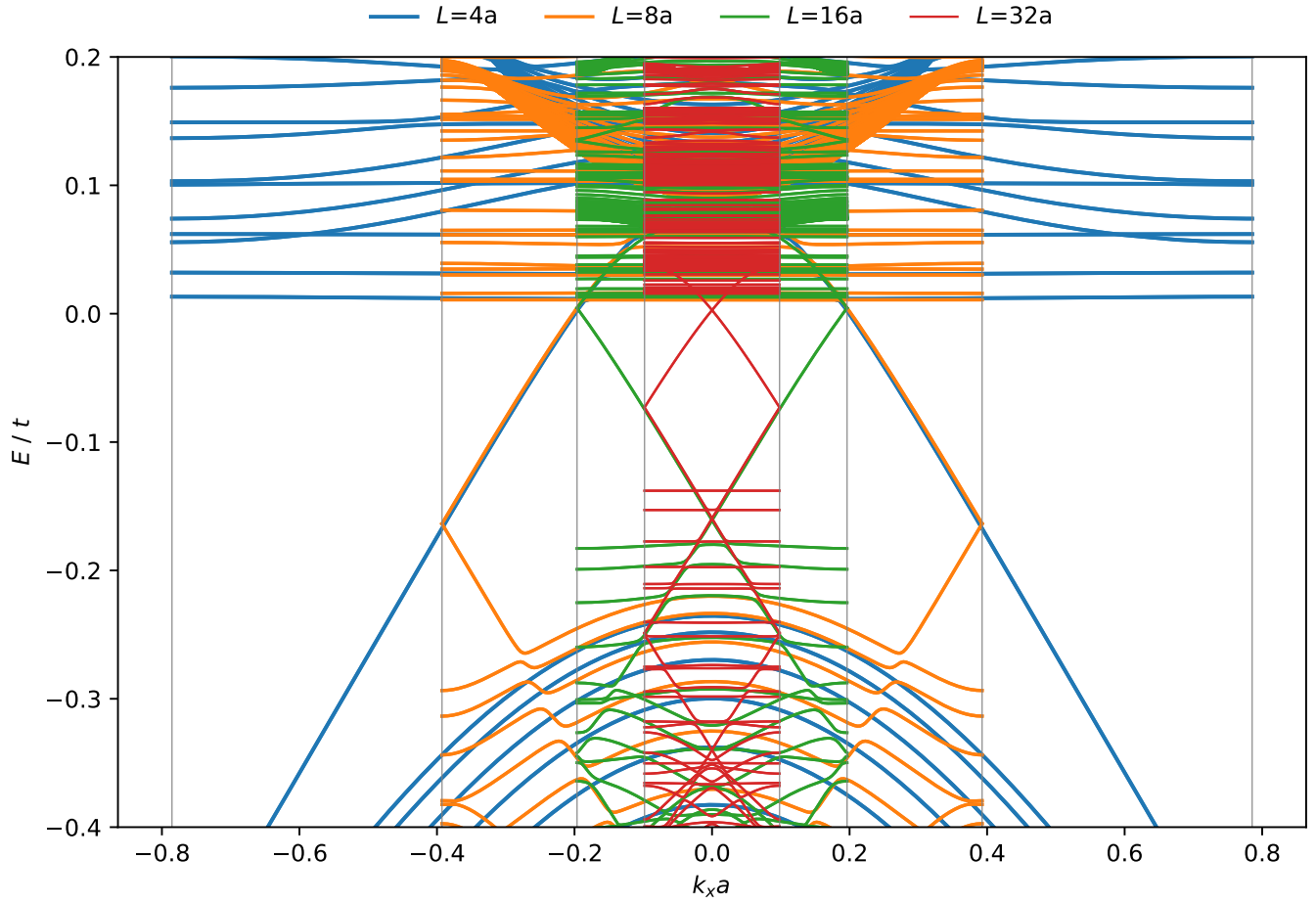


Fig. S27. Band structure of a ribbon configuration for a model including all parameters: next-nearest neighbour (NNN) hoppings, an effective mass term, and spin-orbit coupling (SOC). Bands near $k_x a = 0$ are plotted for SL periodicities $L = 4a, 8a, 16a,$ and $32a$. The width of the ribbon is $W = 40a$. The NNN hopping parameter $t' = -0.5t$, the mass term $U = 0.3t$, and the SOC strength $t_{\text{SOC}} = 0.08t$.